trapping inhibiting bpy–bpy electron transfer occurs by medium-frequency, bpy-based vibrations with $2\chi_M \simeq 2700$ cm^{-1}, low-frequency, apparently Ru–N based modes with $2\chi_L \simeq 1000$ cm^{-1}, and solvent modes with $2\chi_S \approx 1000$ cm^{-1}.[15,43] The χ values are 4 times the classical vibrational trapping energies, and the factor of 2 includes contributions from both ligands for the bpy–bpy electron-exchange process. It is interesting to note that using these values gives a classical energy of activation of $E_a \approx 1200$ cm^{-1}, which is near the experimental value of $\sim$900 cm^{-1} found for bpy–bpy electron transfer in $Fe(bpy)_2(bpy^{-\cdot})^+$.[17] Given the evidence for vibrational trapping, if electronic coupling between ligands is sufficiently small, localization is expected to occur.

However, the situation with regard to the solvent dependence of absorption bands is quite different.[15] Here the optical excitation ($\sim 10^{15}$ s) is short on the time scales for equilibration of the intramolecular modes and of the low-frequency solvent polarization modes. As a consequence, in the excited state, the intramolecular and low-frequency solvent orientational modes at each ligand are those appropriate for the symmetrical ground state. Only the electronic polarization of the solvent medium (D_{op}) can respond to the excitation process. Because this instantaneously follows the electron distribution of the solute, it would not seem to provide a barrier to the bpy–bpy electron-exchange process. However, it does favor a localized excited state over a delocalized one because of the added dipole solvation energy. The variation of absorption band energies with D_{op} establishes this quite clearly.[15]

The observation of excitation localized to a single ligand remains a reasonable observation even in the absence of significant vibrational trapping as long as electronic coupling between the ligands is small. In the absence of any trapping, the frequency of the redistribution of the exchanging electron from one ligand to another is given by $\nu_{et} \approx 4V/h$, where V is the delocalization or resonance energy,[44] and statistical effects are not included. Even with $V = 800$ cm^{-1} (0.1 V), ν_{et} is still $\sim 10^{14}$ s^{-1} and electron hopping between ligands would be too slow to couple significantly with the optical excitation. Actually, it is interesting to note that if V were of the magnitude mentioned above, the excited state could be "delocalized" for a short time period following excitation but before the processes leading to vibrational equilibration occur.

It might be argued that the situation is different in a glass or in the solid state, where orientational correlation times for the surrounding trapping dipoles of the medium are restricted and may be long on the time scale for excited-state decay. However, even in the absence of medium trapping, vibrational trapping by intramolecular vibrational modes does exist. The time scale for an individual molecular emission event is rapid on the vibrational time scale. As is the case for light absorption, even in the absence of vibrational trapping, relatively strong electronic coupling between bpy ligands would be required for interligand electron hopping to become competitive with the emission process.

Acknowledgments are made to the Department of Energy under Grant no. DAAG29-79-K-0111 for support of this research and to the Morehead Foundation for generous fellowship support of E.M.K. We also wish to thank Dr. H. Yersin for a copy of ref 32 in advance of publication.

Registry No. $Ru(bpy)_3^{2+}$, 15158-62-0; $Os(bpy)_3^{2+}$, 23648-06-8.

(44) Duke, C. B. In "Tunneling in Biological Systems"; Chance, B., et al., Eds.; Academic Press: New York, 1979; pp 31–65.

Contribution from the Department of Chemistry, Indian Institute of Technology, Madras 600 036, India

EPR, Magnetic, and Structural Investigations on the Weak-Exchange Heisenberg Linear Chain Bis(*N*-methylphenazinium) Bis(dicyanoethenedithiolato)cuprate(II), $[(NMP)_2][Cu(mnt)_2]$

P. KUPPUSAMY, B. L. RAMAKRISHNA, and P. T. MANOHARAN*

Received November 22, 1983

The title compound $[(NMP)_2][Cu(mnt)_2]$ crystallizes in the monoclinic space group $P2_1/n$ with $a = 11.417$ (2) Å, $b = 8.126$ (2) Å, $c = 17.674$ (7) Å, $\beta = 92.11$ (2)°, and $Z = 2$. The structure, including H, was solved by Patterson and Fourier methods and refined by full-matrix least squares to $R = 0.048$, based on 1944 observations. The compound forms a kind of mixed stack with a donor–acceptor sequence DAD–DAD along the a axis. The static susceptibility measurements showed the exchange to be weak. Single-crystal EPR in the ac^* plane, where the two sites are magnetically equivalent, showed single exchange-narrowed Lorentzian lines with hyperfine dominated line width. The relative magnitudes of various Hamiltonians are $\mathcal{H}_{Zee} > \mathcal{H}_{ex} > \mathcal{H}_{hyp} > \mathcal{H}_{dip}$. The angular dependence of the line width in the ac^* plane along with the computed second moments was used to evaluate the high-temperature Fourier components of the autocorrelation function $C(t)$ and $C^2(t)$. The computed nonsecular components were shown to follow from either the Blume–Hubbard model with $\hat{J} = 2100$ G or from the Anderson–Weiss model with $J = 1175$ G.

Introduction

The metal dithiolate complexes $[M(S_2C_2R_2)_2]^{n-}$ where R = CN, CF_3, etc., are a class of interesting compounds that exhibit low-dimensional cooperative phenomena[1,2] associated with their columnar crystallographic packing. Certain d^7 complexes with M = Ni, Pd, or Pt and R = CN exhibit quite strong apparently one-dimensional exchange coupling with J_o of the order of 10^2 cm^{-1} for dimeric stacks[3] and of the order of unity for regular stacks.[4] On the other hand, the Cu(II) analogue, $[Cu(mnt)_2]^{2-}$ shows quite varied behavior in the small J_o regime. For example, $[(NEt_4)_2][Cu(mnt)_2]$ with J_o

(1) Keller, H. J., Ed. "Low Dimensional Cooperative Phenomena"; Plenum Press: New York, 1975.
(2) Interrante, L. V., Ed. "Extended Interactions between Metal Ions in Transition Metal Complexes"; American Chemical Society: Washington, DC, 1974; ACS Symp. Ser. No. 5.
(3) Weiher, J. F.; Melby, L. R.; Benson, R. E. *J. Am. Chem. Soc.* **1964**, *86*, 4329.
(4) Manoharan, P. T.; Noordik, J. H.; de Boer, E.; Keijzers, C. P. *J. Chem. Phys.* **1981**, *74*, 1980.

0020-1669/84/1323-3886$01.50/0

Table I. Positional ($\times 10^4$) and Thermal Parameters ($\times 10^4$) for $[(NMP)_2][Cu(mnt)_2]$ (Esd's in Parentheses)[a]

atom	x	y	z	U_{11}	U_{22}	U_{33}	U_{12}	U_{13}	U_{23}
Cu	0	0	0	444 (5)	714 (7)	388 (5)	43 (5)	12 (4)	64 (6)
S1	390 (2)	−616 (2)	−1225 (1)	753 (12)	729 (12)	375 (8)	−20 (8)	110 (8)	59 (10)
S2	−655 (2)	2538 (2)	−344 (1)	805 (12)	777 (12)	334 (8)	−73 (8)	17 (7)	116 (10)
C1	−144 (5)	1124 (8)	−1688 (3)	495 (35)	715 (45)	308 (29)	−32 (30)	29 (25)	−55 (33)
C2	−577 (6)	2441 (9)	−1335 (3)	620 (41)	723 (46)	339 (31)	−17 (33)	22 (28)	4 (37)
C3	−143 (6)	1099 (9)	−2509 (4)	584 (41)	734 (50)	466 (39)	0 (34)	56 (30)	34 (36)
C4	−1014 (8)	3822 (11)	−1750 (4)	1297 (73)	858 (61)	332 (37)	−41 (39)	117 (40)	252 (54)
N1	−146 (6)	1061 (9)	−3147 (3)	1020 (50)	1074 (54)	316 (31)	−31 (32)	55 (29)	175 (42)
N2	−1336 (9)	4917 (11)	−2077 (3)	2564 (112)	1126 (64)	396 (36)	100 (43)	162 (49)	814 (74)
N3	3619 (5)	−43 (8)	−972 (3)	654 (34)	693 (40)	450 (30)	155 (30)	82 (24)	−197 (34)
N4	2776 (4)	1829 (8)	218 (3)	503 (31)	704 (40)	498 (31)	−219 (29)	78 (24)	−178 (29)
C5	3193 (6)	1475 (9)	−1086 (3)	573 (40)	644 (48)	477 (36)	−127 (34)	40 (29)	−204 (37)
C6	3214 (7)	2150 (11)	−1848 (4)	772 (50)	879 (62)	503 (39)	−24 (40)	10 (35)	−249 (46)
C7	2769 (8)	3672 (12)	−1997 (4)	931 (63)	897 (65)	705 (51)	42 (48)	28 (44)	−140 (52)
C8	2295 (8)	4614 (11)	−1409 (5)	884 (58)	957 (70)	768 (55)	83 (49)	33 (44)	−46 (50)
C9	2273 (6)	4064 (10)	−676 (4)	649 (47)	700 (55)	811 (53)	−117 (44)	11 (39)	−50 (41)
C10	2727 (5)	2477 (9)	−503 (3)	477 (36)	786 (50)	441 (35)	−124 (35)	63 (27)	−212 (36)
C11	3625 (5)	−665 (9)	−269 (3)	538 (39)	672 (46)	450 (36)	−119 (33)	57 (29)	−204 (34)
C12	4085 (6)	−2280 (10)	−152 (4)	650 (44)	712 (53)	675 (46)	−38 (40)	−18 (36)	−186 (40)
C13	4163 (6)	−2951 (11)	566 (4)	676 (48)	933 (63)	761 (52)	−17 (47)	−24 (39)	249 (45)
C14	3752 (7)	−1970 (13)	1199 (4)	741 (52)	1079 (72)	604 (47)	−88 (47)	−62 (39)	280 (51)
C15	3288 (7)	−407 (11)	1110 (4)	666 (45)	1089 (72)	475 (39)	1 (41)	−26 (33)	309 (46)
C16	3213 (5)	288 (10)	356 (3)	502 (35)	793 (53)	425 (34)	−113 (36)	31 (27)	−247 (39)
C17	2444 (6)	2853 (10)	863 (4)	769 (49)	984 (62)	520 (39)	−389 (40)	193 (35)	−88 (44)

[a] Anisotropic temperature factor is of the form $\exp[-2\pi^2(U_{11}h^2a^{*2} + U_{22}k^2b^{*2} + U_{33}l^2c^{*2} + 2U_{23}klb^*c + 2U_{13}hla^*c^* + 2U_{12}hka^*b^*)]$.

$\simeq 1$ cm^{-1} is semiconducting ($\rho \simeq 10^3$ Ω cm at 400 K)[5] while the corresponding $[NPr_4]$ salt is poorly conducting[6] with $J_0 < 0.0002$ cm^{-1}. The $[NBu_4]$ analogue[7] exhibits a temperature-dependent J_0 that is of comparable magnitude with the nuclear hyperfine interaction. At low temperatures and at certain orientations of the magnetic field, J_0 becomes even smaller than hyperfine coupling, resulting in a multiline spectrum instead of a single exchange-narrowed line. Recently, a first dimeric and nonplanar $[Cu(mnt)_2]^{2-}$ has been reported[8] with the methylene blue cation displaying fine-structure EPR corresponding to triplet excited state. Thus, the chemical flexibility available with this type of system provides a broad range of magnetic and electric properties.

From a theoretical point of view, such systems also provide an understanding about the spin dynamics in the weak-exchange regime. Though J_0 is most often determined from static susceptibility measurements, for weak-exchange regime EPR is a more sensitive probe particularly when dealing with very small interchain interactions or interplane coupling. Soos et al.[9] have studied the spin dynamics associated with $[Cu(NH_3)_4][PtCl_4]$ (CTP) where the isotropic exchange falls conveniently between X- and Q-band frequencies and evaluated the high-temperature Fourier components of the two-spin and four-spin correlation functions that compared successfully with those obtained by using theoretical models such as those of Blume–Hubbard[10] and Anderson–Weiss.[11]

In this paper we report our studies on the exchange interaction in bis(*N*-methylphenazinium) bis(dicyanoethenedithiolato)cuprate(II), $[(NMP^+)_2][Cu(mnt)_2]^{2-}$ (dicyanoethenedithiolate is often called maleonitriledithiolate, mnt^{2-}). This system has a smaller exchange interaction compared to the Zeeman frequencies but still strong enough to average out the dominating hyperfine splitting.

Experimental Section

(i) Preparation of Compounds. $Na_2(mnt)$ was prepared according to the reported[12] procedure. A 310-mg sample of $CuSO_4 \cdot 5H_2O$ was dissolved in 3 mL of water, and the resultant mixture was added in drops with stirring to an aqueous methanolic solution (1:1 v/v, 10 mL) containing 0.5 g of $Na_2(mnt)$. The dark brown solution was filtered, and 1.0 g of $NMP^+CH_3SO_4^-$ (Aldrich Chemical Co.) in 2 mL of aqueous methanol was added slowly to the filtrate. A brownish black precipitate was formed immediately. The compound was filtered and washed with 50 mL of water (10-mL portions) and finally with 10 mL of aqueous methanol. The powder was dried in air; yield 600 mg (66%). Anal. Found (calcd): C, 55.32 (55.61); H, 3.06 (3.02); N, 15.18 (15.26).

A portion of the powder was dissolved in acetonitrile, and the resultant mixture was evaporated slowly at 20 °C to give black crystals with well-developed faces.

(ii) Crystal Structure Determination. Unit cell parameters were obtained by least-squares refinement of the θ values of 25 high-angle reflections chosen from diverse regions of reciprocal space. A crystal of size 0.21 × 0.25 × 0.60 mm^3 was chosen for data collection and mounted with the a axis as the spindle (φ) axis. Three-dimensional intensity data were collected on the Enraf-Nonius (CAD-4) diffractometer with graphite-monochromated Mo Kα (λ = 0.71069 Å) radiation. An ω–2θ scan mode was used. The scan width for each reflection was $1.0 + 0.2 \tan\theta$ for the peak and one-fourth of this value on either side for background. A variable scan speed was used with a maximum counting time for each reflection of 60 s. Whenever the counting rate exceeded 50 000 counts/s, a zirconium attenuator was automatically introduced. Two standard reflections from different regions of reciprocal space were measured after every 50 min of exposure time. They remained essentially constant through the entire period of data collection. A total of 1944 unique reflections with $I > 3\sigma(I)$ were considered as observed. The systematic absences ($h0l$ with $h + l$ odd and $0k0$ with k odd) fixed the space group unambiguously as $P2_1/n$. The raw data were corrected for background, variable scan speed, attenuation factor, and Lorentz and polarization effects. No absorption correction was applied. Crystal data at room temperature are a = 11.417 (2) Å, b = 8.126 (2) Å, c = 17.674 (7) Å, β = 92.11 (2)°, V = 1639 $Å^3$, M_r = 734.4, D_{calcd} = 1.488 g cm^{-3}, Z = 2, μ = 0.90 mm^{-1}, and $F(000)$ = 746.

The structure was solved by standard Patterson and Fourier methods and refined by the method of full-matrix least squares with SHELX-76,[13]

(5) Plumlee, K. W.; Hoffman, B. M.; Ratajack, M. T.; Kannewurf, C. R. *Solid State Commun.* **1974**, *15*, 1651.
(6) Plumlee, K. W. Ph.D. Thesis, Northwestern University, 1975.
(7) Plumlee, K. W.; Hoffman, B. M.; Ibers, J. A.; Soos, Z. G. *J. Chem. Phys.* **1975**, *63*, 1926.
(8) Snaathorst, D.; Doesburg, H. M.; Perenboom, J. A. A. J.; Keijzers, C. P. *Inorg. Chem.* **1981**, *20*, 2526.
(9) Soos, Z. G.; Huang, T. Z.; Valentine, J. S.; Hughes, R. C. *Phys. Rev. B: Solid State* **1973**, *8*, 993. Huang, T. Z.; Soos, Z. G. *Phys. Rev. B: Solid State* **1974**, *9*, 4981.
(10) Blume, M.; Hubbard, J. *Phys. Rev. B: Solid State* **1970**, *1*, 3815.
(11) Anderson, P. W.; Weiss, P. R. *Rev. Mod. Phys.* **1953**, *25*, 269. Anderson, P. W. *J. Phys. Soc. Jpn.* **1954**, *9*, 316.
(12) Davidson, A.; Holm, R. H. *Inorg. Synth.* **1971**, *10*, 8.

Table II. Bond Lengths and Bond Angles in $[(NMP)_2][Cu(mnt)_2]$ (Esd's in Parentheses)

	Bond Lengths, Å		
Cu-S1	2.282 (2)	N4-C17	1.509 (9)
Cu-S2	2.269 (2)	C5-C6	1.455 (10)
S1-C1	1.733 (6)	C5-C10	1.431 (9)
S2-C2	1.759 (6)	C5-C7	1.359 (13)
C1-C2	1.342 (7)	C7-C8	1.414 (12)
C1-C3	1.451 (9)	C8-C9	1.327 (11)
C2-C4	1.421 (9)	C9-C10	1.419 (11)
C3-N1	1.128 (9)	C11-C12	1.426 (11)
C4-N2	1.127 (12)	C11-C16	1.442 (9)
N3-C5	1.339 (9)	C12-C13	1.381 (10)
N3-C11	1.341 (8)	C13-C14	1.465 (11)
N4-C10	1.378 (8)	C14-C15	1.383 (13)
N4-C16	1.367 (10)	C15-C16	1.447 (9)
	Bond Angles, deg		
S1-Cu-S2	91.1 (3)	C5-C6-C7	120.2 (6)
Cu-S1-C1	101.0 (4)	C6-C7-C8	120.0 (7)
Cu-S2-C2	101.4 (4)	C7-C8-C9	122.6 (7)
S1-C1-C2	124.1 (5)	C8-C9-C10	118.7 (6)
S2-C2-C1	116.7 (5)	C9-C10-C5	120.3 (5)
C2-C1-C3	119.3 (5)	C5-C10-N4	116.4 (5)
C1-C2-C4	121.2 (5)	N4-C16-C11	118.8 (5)
C1-C3-N1	179.7 (7)	C16-C11-N3	121.1 (5)
C2-C4-N2	179.2 (6)	C16-C11-C12	120.8 (5)
C5-N3-C11	118.4 (5)	C11-C12-C13	120.5 (6)
C10-N4-C16	121.2 (5)	C12-C13-C14	118.4 (6)
C10-N4-C17	119.0 (5)	C13-C14-C15	123.0 (6)
C16-N4-C17	119.9 (5)	C14-C15-C16	118.5 (6)
N3-C5-C10	124.0 (5)	C15-C16-C11	119.1 (5)
C6-C5-C10	118.1 (5)		

Table III. Hydrogen Positional ($\times 10^4$) and Thermal ($\times 10^3$) Parameters for $[(NMP)_2][Cu(mnt)_2]$ (Esd's in Parentheses)

		x	y	z	U_{11}
H1	C6	3695 (41)	1366 (62)	−2237 (26)	103 (15)
H2	C7	2838 (41)	4307 (61)	−2502 (27)	110 (15)
H3	C8	2143 (41)	5909 (61)	−1535 (26)	127 (15)
H4	C9	1977 (41)	4700 (61)	−263 (26)	110 (15)
H5	C12	4385 (40)	−3086 (62)	−617 (26)	101 (15)
H6	C13	4494 (41)	−4226 (61)	652 (26)	108 (14)
H7	C14	3844 (41)	−2472 (62)	1740 (26)	109 (15)
H8	C15	2961 (40)	265 (64)	1589 (26)	99 (14)
H9	C17	2997 (42)	3757 (64)	992 (27)	116 (15)
H10	C17	2664 (44)	2314 (65)	1389 (27)	120 (14)
H11	C17	1680 (42)	2567 (62)	921 (27)	122 (15)

initially with isotropic and then with anisotropic thermal parameters for the non-hydrogen atoms. Final Fourier maps revealed all 11 hydrogen atom positions. The hydrogen atom positions were refined once. Symmetry restrictions on anisotropic temperature parameters for the Cu atom, which is lying in the special position, were applied following the work of Peterse and Palm.[14] The atomic scattering factors for Cu^{2+} were taken from Cromer[15] and for the non-hydrogen atoms from Cromer and Mann.[16] The anomalous dispersion factors were taken from Cromer and Liberman.[17] The H atom scattering factors were taken from Stewart, Davidson, and Simpson.[18] The final R and R_w values are 0.048 and 0.057, respectively, with $w = 0.0330/(\sigma^2(F_o) + 0.1056|F_o|^2)$.

Fractional atomic coordinates of the non-hydrogen atoms with anisotropic thermal parameters are listed in Table I. The numbering of the atoms is shown in Figure 1. Table II contains the relevant bond distances and bond angles. The H positional parameters with isotropic thermal parameters are listed in Table III. Least-squares plane calculations are shown in Table IV.

(13) Sheldrick, G. M. "SHELX-76, Program for Crystal Structure Determination"; University of Cambridge: Cambridge, England, 1976.
(14) Peterse, W. J. A. M.; Palm, J. H. *Acta Crystallogr., Sect. A: Cryst. Phys., Diffr., Theor. Gen. Crystallogr.* **1966**, *A20*, 147.
(15) Cromer, D. T. *Acta Crystallogr.* **1965**, *18*, 104.
(16) Cromer, D. T.; Mann, J. B. *Acta Crystallogr., Sect. A: Cryst. Phys., Diffr., Theor. Crystallogr.* **1968**, *A24*, 321.
(17) Cromer, D. T.; Liberman, D. G. *J. Chem. Phys.* **1970**, *53*, 1891.
(18) Stewart, R. F.; Davidson, E. R.; Simpson, W. T. *J. Chem. Phys.* **1965**, *42*, 3175.

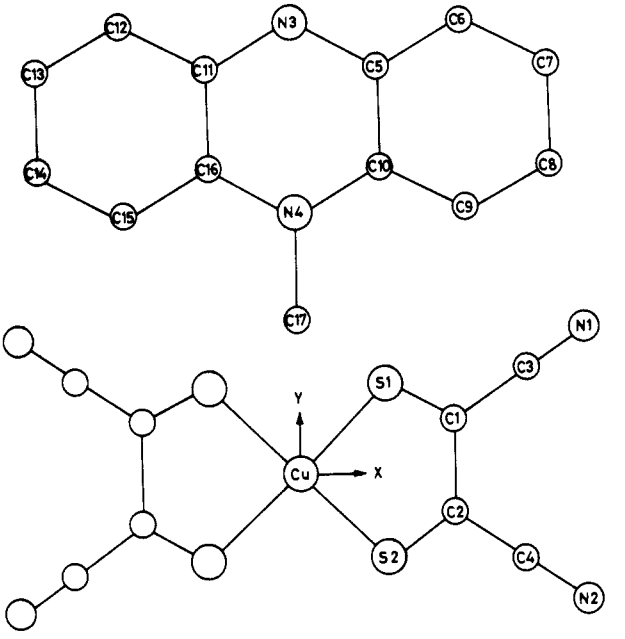

Figure 1. Structural formula of $[(NMP)_2][Cu(mnt)_2]$.

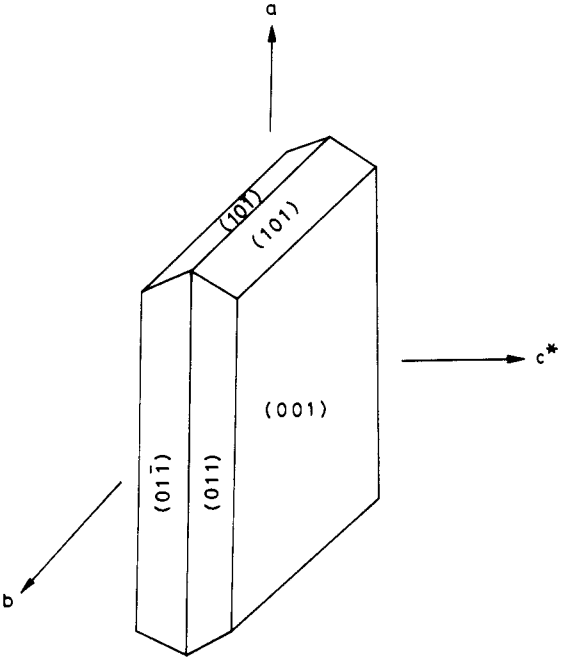

Figure 2. Morphology of $[(NMP)_2][Cu(mnt)_2]$.

(iii) Magnetic and EPR Measurements. The static magnetic susceptibility of powdered sample was measured over the temperature range 4.2–300 K at a field of 18.94 kG. The error in the susceptibility measurement was 1–2% and that in the temperature was ±0.2 K. EPR measurements were made with a Varian E-4 spectrometer at X-band and with a Varian E-112 spectrometer at Q-band frequencies. DPPH was used as a g calibrant. The error in the g value is ±0.002.

The morphology of the crystals used for EPR measurements is shown in Figure 2. Measurements were made with the magnetic field in the *ab*, *bc*, and *ac** planes. All line widths reported here are peak-to peak width of the first derivative of the absorption spectrum, ΔB_{pp}. The error in the line width is ±1.0 G.

Results and Discussion

(i) Crystal Structure. The Cu atoms of the anions occupy the inversion centers at (0, 0, 0) and ($^1/_2$, $^1/_2$, $^1/_2$) such that the CuS_4 core is strictly planar. The $[Cu(mnt)_2]^{2-}$ anion is planar with a mean deviation from the least-squares plane through all the atoms of the anion of 0.065 Å. The $[NMP]^+$ ion is very slightly bent along with the line N–N. The

Table IV. Least-Squares Planes in $[(NMP)_2][Cu(mnt)_2]$[a]

plane 1: Cu, S1, S2, C1, C2, C3, C4, C5, N1, N2
plane 2: $[NMP]^+$ ion as a whole
plane 3: N3, N4, C5, C6, C7, C8, C9, C10
plane 4: N3, N4, C11, C12, C13, C14, C15, C16

plane	*A*	*B*	*C*	*D*
1	−0.9152	0.3984	−0.5981	0.0142
2	−0.9063	0.3877	−0.1680	0.1278
3	−0.9003	0.3933	−0.1862	0.1427
4	−0.9093	0.3873	−0.1522	0.1155

Deviations from Planes, Å

plane 1		plane 2			plane 3		plane 4	
Cu	0.0929	N3	−0.0097	C10	−0.0272	N3	−0.0235	N3	0.0285
S1	−0.0586	N4	−0.0092	C11	−0.0323	N4	0.0301	N4	−0.0078
S2	−0.0285	C5	0.0006	C12	−0.0373	C5	−0.0071	C11	−0.0136
C1	−0.0426	C6	0.0538	C13	0.0028	C6	0.0242	C12	−0.0198
C2	−0.0329	C7	0.0374	C14	0.0372	C7	0.0129	C13	0.0005
C3	0.0024	C8	−0.0164	C15	0.0283	C8	−0.0142	C14	0.0154
C4	−0.0042	C9	−0.0382	C16	−0.0097	C9	−0.0144	C15	0.0070
N1	0.0472								
N2	0.0242								

[a] Equation of the normal to the least-squares plane is $Ax + By + Cz = D$, where x, y, and z are orthogonal coordinates.

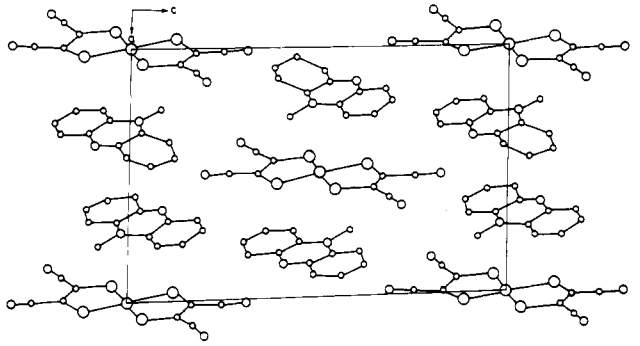

Figure 3. Projection of the packing arrangement of $[(NMP)_2][Cu(mnt)_2]$.

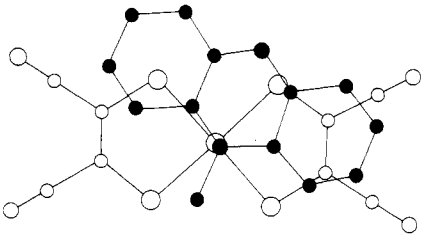

Figure 4. Perpendicular projection of $[NMP]^+$ onto the $[Cu(mnt)_2]^{2-}$ plane.

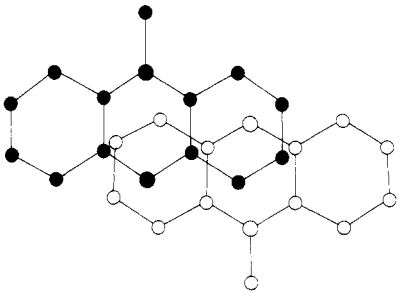

Figure 5. Perpendicular projection of $[NMP]^+$ ion onto the $[NMP]^+$ ion plane of adjacent triads.

least-squares planes through each half of the cation about N–N form an angle of 2.05°, with a maximum deviation from each plane being 0.03 Å (N4) and 0.029 Å (N3), respectively. If a mean plane is calculated through all the atoms of the cation, the maximum deviation is 0.05 Å (C6). The dihedral angle between the two planes about the N–N bond of the cation (2.05°) is comparable to the corresponding ones found in $[(NMP)_2][Ni(mnt)_2]$ (4°)[19] and in $[NMP][Ni(mnt)_2]$ (0.85°).[20]

A projection of the packing arrangement onto the *ac* plane is shown in Figure 3. The packing can be best described as a kind of "mixed stack"[21] along the *a* axis. The anion planes are sandwiched between $[NMP]^+$ planes such that the donor–acceptor sequence is DAD–DAD along the stack axis. The interplanar distance between the cation and the anion within the triad is 3.51 Å while that between two adjacent cations along the *a* axis is 3.33 Å. The corresponding distances in the Ni analogue are 3.48 and 3.35 Å, respectively.[19] A perpendicular projection of an $[NMP]^+$ onto the $[Cu(mnt)_2]^{2-}$ plane is shown in Figure 4. The mode of overlap of two $[NMP]^+$ ions of adjacent triads is shown in Figure 5. It should be noted that the $[NMP]^+$–$[NMP]^+$ overlap between adjacent triads is similar to that found in $[NMP][Ni(mnt)_2]$[20] but is quite different from that in $[(NMP)_2][Ni(mnu)_2]$,[19] even though the interplanar distance is almost the same.

The bond parameters in the $[Cu(mnt)_2]^{2-}$ anion of the present compound compare well with those reported for similar systems.[5,7] The bond parameters in $[NMP]^+$ are in good agreement with those found in $[(NMP)_2][Ni(mnt)_2]$ and $[NMP][Ni(mnt)_2]$, establishing the fact that the cation is $[NMP]^+$ and not $[HMP]^+$ (*N*-hydro-*N*-methylphenaziniumyl cation).[22] Further, no H atom bound to N3 could be found in the difference Fourier map, which clearly revealed all other H positions.

There are two magnetically inequivalent anions in the unit cell, and the normals to the anion chelate planes subtend an angle of ±68.6° with respect to the symmetry axis, *b*.

(ii) Magnetic Susceptibility. The susceptibility data are corrected for a diamagnetic contribution to -481×10^{-6}

(19) Endres, H.; Keller, H. J.; Moroni, W.; Nothe, D. *Acta Crystallogr., Sect. B: Struct. Crystallogr. Cryst. Chem.* **1979**, *B35*, 353.
(20) Kuppusamy, P.; Mahadevan, C.; Seshasayee, M.; Manoharan, P. T. *J. Crystallogr. Spectrosc. Res.*, in press.
(21) Soos, Z. G.; Keller, H. J. "Chemistry and Physics of One-Dimensional Metals"; Keller, H. J., Ed.; NATO ASI Series: New York, 1977; No. 25.
(22) Morosin, B. *Acta Crystallogr., Sect. B: Struct. Crystallogr. Cryst. Chem.* **1978**, *B34*, 1905.

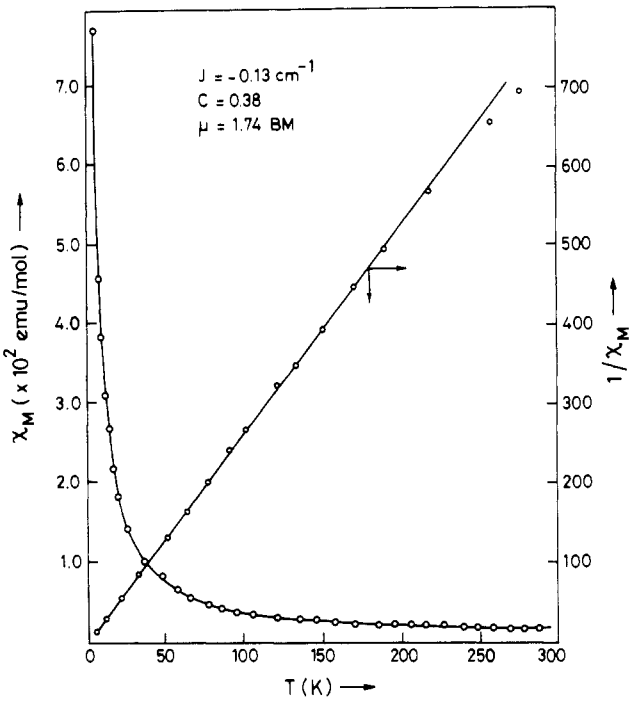

Figure 6. Corrected molar susceptibility χ_M and χ_M^{-1}, as a function of temperature. In the χ_M vs. T plot, the solid line is the calculated one using the Heisenberg linear-chain model with $J = -0.13$ cm^{-1} whereas the circles are experimental points. In the χ_M^{-1} vs. T plot, the solid line is that for $\chi_M^{-1} = T/0.38$ and the circles are experimental points.

cgsu/mol with Pascals constants taken from ref 23. The variation of susceptibility with temperature is shown in Figure 6. The fact that there is no reduction in the susceptibility even down to 4.2 K means that the J_0 value is lower than 4.2 K. The susceptibility exhibits a Curie–Weiss dependence with negligible Weiss correction. The whole data set can be fit into the expression $\chi_M^{-1} = (T + 0.0)/0.38$. The Curie–Weiss constant (0.38) is only 5% less than the spin-only value of 0.40.

Assuming the Heisenberg linear-chain model of $S = {}^1/_2$ spins, the exchange Hamiltonian is given by

$$\mathcal{H}_{ex} = -2J_0\sum S_i \cdot S_{i+1} \quad (1)$$

The data were fit into the analytical expression developed by Hall and Hatfield.[24] Their expression is

$$\chi_M = \frac{N\bar{g}^2\beta^2}{kT}\,\frac{A + Bx^{-1} + Cx^{-2}}{1 + Dx^{-1} + Ex^{-2} + Fx^{-3}} \quad (2)$$

where $x = J_0/kT$, $A = 0.25$, $B = 0.149445$, $C = 0.30094$, $D = 1.9862$, $E = 0.68854$, and $F = 6.0626$. The best fit was obtained by minimizing the error function

$$F(\bar{g},J_0) = \frac{1}{N}\sum_N(\chi_i^{\text{exptl}} - \chi_i^{\text{calcd}})^2 T_i^2 \quad (3)$$

to give $J_0 = -0.064$ cm^{-1} and $\bar{g} = 2.043$ with the error function F better than 0.0002. The agreement between calculated and experimental susceptibility values is shown in Figure 6. Taking $J = 2J_0$ we obtain a value of about 1200 G for exchange interaction in this system.

(iii) g Tensor. Two EPR lines were observed in both *ab* and *bc* planes while only one line in the *ac** plane (by symmetry) at X-band. The same pattern was observed at Q-band except

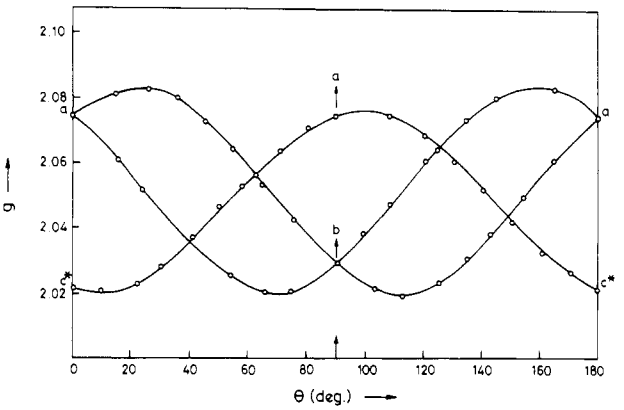

Figure 7. Angular variation of g in the *ab* and *ac** planes. The solid curves are the simulated ones from the crystal direction cosines, and the circles are experimental points.

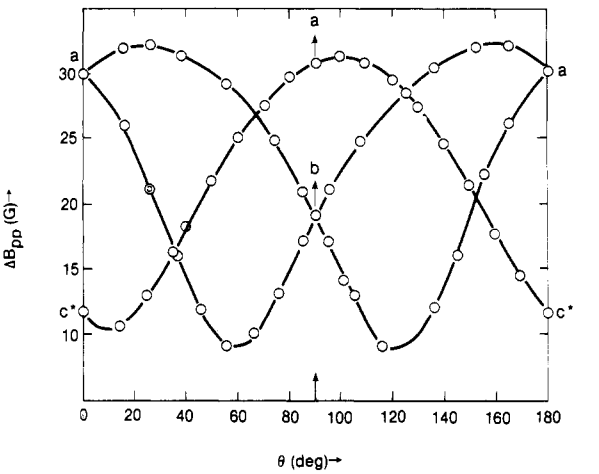

Figure 8. Angular variation of line width, ΔB_{pp}, in the *ab* and *ac** planes.

that the two lines that were not well resolved for most of the orientations at X-band could be resolved well at Q-band. The line position (g) as well as line width (ΔB_{pp}) variations with the magnetic field directions are shown in Figures 7 and 8 for *ab* and *ac** planes at X-band. A simple diagonalization procedure yielded the following principal values for g: $g_{xx} = 2.024$, $g_{yy} = 2.017$, and $g_{zz} = 2.085$. These values are in close agreement with the g values reported[25] for $[(NBu_4)_2][Cu(mnt)_2]$ diluted in the corresponding Ni(II) lattice ($g_{xx} = 2.026$, $g_{yy} = 2.023$, $g_{zz} = 2.086$). The isofrequency plot simulated by using crystal structure **g**-tensor directions and doped g values matches very well with the experimental values shown in Figure 7. This clearly shows that the interchain exchange (between inequivalent chains), if at all, is very small because there is hardly any shift in the line positions in the *ab* plane.

(iv) Line Width Analysis. The angular dependence of line width in the *ab* and *ac** planes is shown in Figure 8. In both planes the line width follows g variation, showing the predominant contribution of hyperfine broading. The fact that no change in line width was observed at Q-band suggests that the exchange frequency $\omega_e = J/\hbar$ must be smaller than both spectrometer frequencies, ω_0. Hence, in the present system the relative magnitudes of various spin Hamiltonians are $\mathcal{H}_{Zee} > \mathcal{H}_{ex} > \mathcal{H}_{hyp} > \mathcal{H}_{dip}$. Cooling the crystal down to 20 K with $\vec{B}\|a$ and with $\vec{B}$ making an angle of 75° with b in the *bc* plane did not show any appreciable change in line width. Also measurements were carried out down to 4 K in the *ab* plane

(23) König, E.; König, G. "Magnetic Properties of Coordination and Organometallic Transition Metal Compounds"; Hellwege, K. H., Hellwege, A. M., Eds.; Springer-Verlag: Berlin, 1976; Landölt-Börnstein New Series, Vol. II/8.
(24) Hall, J. W. Ph.D. Thesis, University of North Carolina, 1977. Hatfield, W. E. *J. Appl. Phys.* **1981**, *52*, 1985.
(25) Maki, A. H.; Edelstein, N.; Davidson, A.; Holm, R. H. *J. Am. Chem. Soc.* **1964**, *86*, 4580.

at an orientation where the two lines are separated maximum and no change in line width could be observed. The line-shape analysis for the line with $\vec{B} \| a$ and $\vec{B}$ at 100° away from a in the ac^* plane revealed it to be Lorentzian in shape (within experimental error).

Soos et al.[9] have studied [Cu(NH$_3$)$_4$][PtCl$_4$], a system where $\mathcal{H}_{Zee}^{Q} > \mathcal{H}_{ex} > \mathcal{H}_{Zee}^{X} > \mathcal{H}_{hyp} \approx \mathcal{H}_{dip}$ and evaluated the high-temperature Fourier components of two- and four-spin correlation functions using Blume–Hubbard[10] and Anderson–Weiss[11] models. But, in the literature there has not been any work, to our knowledge, about systems with $\mathcal{H}_{Zee} > \mathcal{H}_{ex} > \mathcal{H}_{broadening}$ and so we attempted to use the above models with the computed local field second moments[26] to get the Fourier components of the spin correlation functions as well as the magnitude of the isotropic exchange coupling constant.

By exchange-narrowing theories,[11,27] the line contour of the main EPR line is given by

$$I(\omega - \omega_0) = \frac{1}{2\pi}\int_{-\infty}^{+\infty} \varphi(t) \exp[i(\omega - \omega_0)t]\, dt \qquad (4)$$

where $\varphi(t)$, the relaxation function for the decay of the transverse magnetization, is

$$\varphi(t) = \exp\left[-\int_0^{\tau} (t - \tau)\, \psi(\tau)\, d\tau\right] \qquad (5)$$

with the local field correlation function

$$\psi(\tau) = \langle \Delta\omega(\tau)\, \Delta\omega(0) \rangle \qquad (6)$$

and $\psi(0)$, given by the second frequency moment. When the exchange is much stronger than the broadening mechanisms (as in the present case), i.e. when $t \gg \tau$, $\varphi(t)$ can be approximated by

$$\varphi(t) \approx \varphi(0) = \exp\left[-t \int_0^{\infty} \psi(\tau)\, d\tau\right] \qquad (7)$$

which gives

$$\Gamma = \int_0^{\infty} \psi(\tau)\, d\tau \qquad (8)$$

where Γ is the half-width at half-height. This approximation is valid when (i) $\tau(\simeq \hbar/J) \ll \Gamma^{-1}$, (ii) $\psi(\tau)$ is integrable, which is not the case, for example, in one-dimensional spin diffusion, when $\psi(\tau) \propto \tau^{-1/2}$, and (iii) the line shape is close to Lorentzian.

The hyperfine coupling involves two-spin correlation functions, and in the high-temperature limit its contribution to line width is given by

$$\Gamma_h = a^{(0)}\, g(0) + a^{(1)}\, g(\omega) \qquad (9)$$

where $a^{(0)}$ and $a^{(1)}$ are the secular and nonsecular hyperfine second moments and $g(\omega)$ are the Fourier components of the autocorrelation function

$$2g(\omega) = \int_{-\infty}^{+\infty} \exp(i\omega t)\, C(t)\, dt \qquad (10)$$

On the other hand, the dipolar interaction involves four-spin correlations, and in the strong decoupling limit, the dipolar contribution to line width is given by

$$\Gamma_d = M_2^{(0)} f(0) + M_2^{(1)} f(\omega) + M_2^{(2)} f(2\omega) \qquad (11)$$

where $M_2^{(0)}$, $M_2^{(1)}$, and $M_2^{(2)}$ are respectively the secular ($\Delta m = 0$) and nonsecular ($\Delta m = \pm 1, \pm 2$) dipolar second moments and $f(\omega)$ are the Fourier components of the square of the autocorrelation function, $C^2(t)$.

$$2f(\omega) = \int_{-\infty}^{+\infty} C^2(t) \exp(i\omega t)\, dt \qquad (12)$$

(26) McGregor, K. T.; Soos, Z. G. *J. Chem. Phys.* **1976**, *64*, 2506.
(27) Kubo, R.; Tomita, K. *J. Phys. Soc. Jpn.* **1954**, *9*, 888.

Table V. Local Fields in the ac^* Plane (10^3 G^2)

direction of $\vec{B}$ (θ, deg)	hyperfine second moment[a]		dipolar second moment[b]		
	secular	nonsecular	secular	nonsecular	
	$\Delta m = 0$	$\Delta m = \pm 1$	$\Delta m = 0$	$\Delta m = \pm 1$	$\Delta m = \pm 2$
0 (c^*)	2.79	15.15	2.60	2.14	1.89
30	6.09	9.34	2.79	1.84	1.97
60	19.82	4.47	2.94	1.66	2.09
90 (a)	29.90	2.79	2.59	2.11	2.10
120	26.87	3.25	2.82	1.95	2.06
150	13.52	5.90	2.99	1.78	1.99
180 (c^*)	2.79	15.15	2.60	2.14	1.89

[a] $g_\parallel = 2.085$, $g_\perp = 2.021$, $A_\parallel = 166$ G, $A_\perp = 41$ G. [b] $g = 2.043$ and spins quantized along $g\vec{B}$.

Table VI. Fourier Components of Spin Correlation Functions $C(t)$ and $C^2(t)$ (10^{-3} G^{-1})

Fourier components ($\omega = 9.47$ GHz)	B–H model ($\hat{J} = 2100$ G)	A–W model ($J = 1175$ G)	exptl
$g(0)$	0.95	0.85	0.64 ± 0.03
$g(\omega)$	0.061	0.061	0.07 ± 0.01
$f(0)$	0.65	0.60	2.79 ± 0.40
$f(\omega)$	0.145	0.161	0.15 ± 0.01
$f(2\omega)$	0.006	0.003	0.005 ± 0.005

The experimental peak-to-peak line width, ΔB_{pp}, is related to the local field correlation as

$$(3^{1/2}/2)\Delta B_{pp} = \Gamma_{total} = a^{(0)}\, g(0) + a^{(1)}\, g(\omega) + M_2^{(0)} f(0) + M_2^{(1)} f(\omega) + M_2^{(2)} f(2\omega) \qquad (13)$$

The angular dependence of Γ thus provides equations in which the Fourier components, $g(0)$, $g(\omega)$, ..., are the only unknowns.

Since only in the ac^* plane the magnetic equivalency of all the sites is present, we have chosen this plane for analysis. The computed[9,26] local field contributions for a few selected orientations are given in the Table V. Although it is known that the nonsecular contributions will be negligible for $\mathcal{H}_{Zee} \gg \mathcal{H}_{ex}$, we have explicitly included them also in the evaluation of Fourier components. Using the X-band line width data in the ac^* plane (18 values at 10° intervals) a consistent solution for these coefficients was obtained by using fitting procedure. The values thus obtained are listed in Table VI.

The Blume–Hubbard high-temperature approximation[10] for $C(t)$ for $S = {}^1/_2$ is

$$C_{BH}(t) = \cosh^{-2}(\tfrac{1}{2}\hat{J}t) \qquad (14)$$

where $\hat{J}$ is the rms exchange ($\hat{J} = 2^{1/2}J$). The Fourier components of $C_{BH}(t)$ and $C_{BH}^2(t)$ are

$$g_{BH}(x) = \hat{J}(x/\sinh x) \qquad (15)$$

and

$$f_{BH}(x) = (4/3\hat{J})(x/\sinh x)[1 + (x/\pi)^2] \qquad (16)$$

where x, the scaled frequency, is $\pi\omega/\hat{J}$. For $\omega = 9.47$ GHz (3380 G, X-band) and $\hat{J} = 2100$ G the computed Fourier components are given in Table VI.

On the other hand, the Anderson–Weiss proposal[11] of Gaussian $C(t)$ for exchange narrowing is

$$C_G(t) = \exp[-\tfrac{1}{4}\pi\omega_e^2 t^2] \qquad (17)$$

$\omega_e \simeq J$ leads to the following expressions for $g(\omega)$ and $f(\omega)$:

$$g_G(\omega) = (1/\omega_e) \exp[(-1/\pi)(\omega^2/\omega_e^2)] \qquad (18)$$

$$f_G(\omega) = (1/(2\omega_e)^{1/2}) \exp[(-1/2\pi)(\omega^2/\omega_e^2)] \qquad (19)$$

The X-band Fourier components calculated based on this

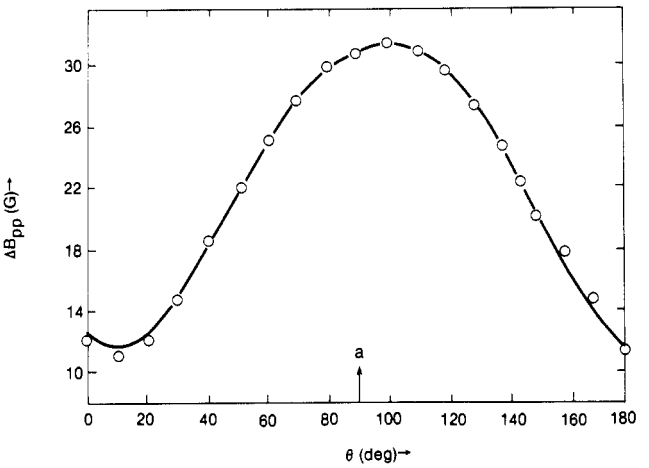

Figure 9. Experimental (solid line) and calculated (O) line widths in the *ac** plane. The calculated line widths are based on Blume–Hubbard $C_{BH}(t)$ with $\hat{J}$ = 2100 G and with Fourier components $g(0) = 0.64 \times 10^{-3}$, $g(\omega) = 0.061 \times 10^{-3}$ G^{-1}, $f(0) = 2.79 \times 10^{-3}$ G^{-1}, $f(\omega) = 0.145 \times 10^{-3}$ G^{-1}, and $f(2\omega) = 0.006 \times 10^{-3}$ G^{-1} at ω = 9.47 GHz.

model are again given in Table VI.

Both models give almost the same values for nonsecular spin correlation functions. They also compare well with the experimental values. But secular spin correlations are not predicted correctly by these models. In the present system, $g(0)$ is overestimated and $f(0)$ is largely underestimated whereas in $[Cu(NH_3)_4][PtCl_4]$ both $g(0)$ and $f(0)$ are underestimated.[9] The Q-band (ω = 35 GHz) nonsecular Fourier components calculated by using the above models are negligibly small. This is to be anticipated as the Zeeman frequency is much larger than the exchange frequency.

However, one point is worth mentioning. The larger $f(0)$ clearly reflects the one-dimensional behavior as expected from the crystal structure. But, the smaller $g(0)$ is puzzling. The autocorrelation function $C(t)$ is usually normalized at $t = 0$, as in eq 14 and 17 for the two models. Now, the conditions $C(t) \leq 1$ lead to $f(0) < g(0)$ quite independently of any model, including those with diffusive tails. The opposite experimental conclusion could be due to (1) failure of the decoupling approximations (we are thankful to the reviewer for pointing this out), (2) not separating into intrachain and interchain dipolar second moments, or (3) the use, most probably, of six or seven equations for five unknowns. The observation of a Lorentzian line shape indicates sufficient interchain interaction, if not enough to mask the presence of two separate resonances for the two sites. This point may support the second reason cited above.

The exchange values obtained from these models ($J \simeq 1500$ G for the B–H model and $J \simeq 1200$ G for the A–W model) also agree reasonably well with that obtained from susceptibility measurements ($J \simeq 1250$ G). The calculated line width from the B–H model is compared with the experimental line widths in Figure 9 for the *ac** plane where both the sites are magnetically equivalent. The rather large value of $g(0)$ and $f(0)$ are surprising and may suggest one-dimensional exchange through $[NMP]^+$ ions between successive $[Cu(mnt)_2]^{2-}$ anions.

Conclusion

The salt $[(NMP)_2][Cu(mnt)_2]$ crystallizes in a mixed stack with a donor–acceptor sequence of the type DAD–DAD along the *a* axis. Since each anion is sandwiched between two cations, the exchange interaction within a chain is weak ($J \simeq 1200$ G) in spite of it having described as a linear Heisenberg chain. In addition, the prediction of the correct order to the exchange coupling through EPR line width in line with the susceptibility prediction has been found to be fairly successful by using the existing theories for weak exchange.

Acknowledgment. This work was supported by a scheme from the Department of Science and Technology, Government of India, New Delhi, for which we are grateful. P.K. also expresses his thanks to the UGC, New Delhi, and Pachaiyappa's College, Madras, for the award of FIP fellowship.

Registry No. $[(NMP)_2][Cu(mnt)_2]$, 92241-56-0.

Supplementary Material Available: A listing of the structure factor amplitudes for $[(NMP)_2][Cu(mnt)_2]$ (9 pages). Ordering information is given on any current masthead page.

Contribution from the Department of Chemistry, University of Cincinnati, Cincinnati, Ohio 45221

Infrared Matrix Isolation Study of Intermediate Molecular Complexes: Complexes of GeF_4 with Oxygen-Containing Bases

ANGELA M. WALTHER and BRUCE S. AULT*

Received February 17, 1984

The codeposition of GeF_4 with a variety of oxygen-containing bases, through either the twin-jet or single-jet mode into argon matrices, has led to the formation of intermediate 1:1 complexes. The species of $H_2O{\cdot}GeF_4$, $CH_3(H)O{\cdot}GeF_4$, $(CH_3)_2O{\cdot}GeF_4$, $CD_2O{\cdot}GeF_4$, and $(CH_3)_2CO{\cdot}GeF_4$ were each identified and characterized spectroscopically. The infrared spectra indicate that all are bound through the oxygen to the germanium center. The observed spectral features could be divided into two categories, corresponding to perturbed acid and base subunit vibrations. These indicate that the structure is near a trigonal bipyramid, as was observed for the corresponding ammonia complex, although the lower symmetry of the base precludes a C_3 axis in the complex. The position of the antisymmetric Ge–F stretching mode of the "near-equatorial" fluorines was shown to correlate with the proton affinity of the base, as anticipated and as observed previously for the analogous SiF_4 complexes. In addition, with use of the degree of perturbation of the base subunit as a measure, the spectra indicate that GeF_4 forms substantially stronger complexes with these bases than does SiF_4.

Introduction

Lewis acid–base adducts and the nature of the coordinate bond have been of interest to chemists for a number of years, and many examples are known, particularly for strong acids and bases.[1] Within the past few years, the matrix isolation technique has been applied successfully to study less stable complexes, either those that are only weakly bound or those

(1) Jensen, W. B. "The Lewis Acid-Base Concepts: An Overview"; Wiley-Interscience: New York, 1980, and references therein.

0020-1669/84/1323-3892$01.50/0